Compact Low Loss Mid-Infrared Wavelength-Flattened Directional Coupler (WFDC) for Arbitrary Power Splitting Ratio Enabled by Rib Waveguide Dispersion Engineering

Bowei Dong, *Student Member, IEEE*, Xianshu Luo, Ting Hu, Tina Xin Guo, Hong Wang, Dim-Lee Kwong, Patrick Guo-Qiang Lo, and Chengkuo Lee

***Abstract*—We design, fabricate, and characterize a novel type of wavelength-flattened directional coupler (WFDC) working in the mid-infrared (MIR) based on the physics of rib waveguide dispersion. In the silicon-on-insulator rib waveguide WFDC devices with length <20 μm, a 6-fold enhancement and a 4-fold enhancement in the operation bandwidth compared with the conventional directional coupler are achieved for 50:50 (± 5) and 100:0 (-2) power splitting ratio, respectively, with an average low excess loss of -0.52 ± 0.18 dB/device. To the best of our knowledge, our device is the first WFDC working in the MIR and the first WFDC that possesses low excess loss, CMOS compatibility and compactness simultaneously, while the novel mechanism could be adopted easily to realize arbitrary power splitting ratio. Our work could serve as a promising component for light routing and power splitting in broadband MIR applications, such as MIR spectrometer sensing systems. In addition, the proposed novel mechanism could be adopted for near-infrared as well to achieve better WFDC performance.**

***Index Terms*—Dispersion, optical coupling, optical losses, optical waveguides, photonic integrated circuits, silicon photonics.**

I. Introduction

SENSORS are essential in the modern society for providing functionalities including environmental monitoring, industrial control, homeland security inspection, and pharmaceutical diagnostics. To thoroughly monitor surroundings or specific subjects, billions of sensors are demanded. Thus, integrated sensors with small footprints, low power consumption, and low cost are desired.

Mid-infrared (MIR) nanophotonics sensors are promising in fulfilling this goal [1]–[5]. MIR, which is part of the electromagnetic spectrum with wavelength ranging from 2 μm to 20 μm [6], contains the fingerprints of many common environmental gases and biological molecules such as C-H, C = C, O-H, glucose, and DNA [7]. This would enable label free and damage free sensors [8]. Moreover, the mature complementary metal-oxide-semiconductor (CMOS) fabrication techniques can be leveraged to achieve economical millimeter-scale integrated sensors. The successful utilization of CMOS fabrication techniques for near-infrared (NIR) nanophotonics in tele-communication bands has demonstrated the feasibility [9]–[12].

In MIR nanophotonics sensing systems, a broadband light source is required for the spectrum analysis which identifies the fingerprints of different species. Consequently, wavelength-flattened (WF) devices are necessary to function in accordance with the broadband light source. However, to the best of our knowledge, there is no report on MIR WF directional coupler (DC) which is a key component for light routing and power splitting [13].

Conventional DC consists of two slightly spaced fully etched waveguides. Owing to the evanescent wave coupling, light transfers between the two waveguides. Nonetheless, the power transfer is sensitive to wavelength. There are several attempts based on different physics to achieve WFDC for NIR. These might stimulate inspirations for the design of WFDC for MIR. In 1989, an early theoretical work tried to alleviate the wavelength dependence of the DC coupling coefficient by determining the optimal coupling gap [14]. This method is only effective for the highest power splitting ratio, i.e., 100:0. Following this idea, there were several demonstrations working for other power splitting ratio by breaking the symmetry of the DC so that the highest power splitting ratio shifted away from 100:0 [15]–[18]. A 7-fold enhancement in the operation bandwidth compared to the conventional DC is achieved in 2014 [19]. However, it is difficult to achieve arbitrary power splitting ratio based on this mechanism due to the tedious design process and the low

Manuscript received September 28, 2017; revised January 5, 2018; accepted February 28, 2018. Date of publication March 8, 2018; date of current version April 5, 2018. This work was supported in part by the Research Grant of NRF-CRP15-2015-02 at the National University of Singapore, Singapore, and in part by the Research Grant of NRF-CRP12-2013-04 at Nanyang Technological University, Singapore. *(Corresponding authors: Xianshu Luo; Chengkuo Lee.)*

B. Dong and C. Lee are with the Department of Electrical and Computer Engineering, the Center for Intelligent Sensors and MEMS, and the Graduate School for Integrative Science and Engineering, National University of Singapore, Singapore, 117576 (e-mail: dongbowei@u.nus.edu; elelc@nus.edu.sg).

X. Luo, T. Hu, and P. G.-Q. Lo are with the, Institute of Microelectronics, Agency for Science, Technology and Research, Singapore, 138634 (e-mail: luox@ime.a-star.edu.sg; hut@ime.a-star.edu.sg; logq@ime.a-star.edu.sg).

T. X. Guo and H. Wang are with the School of Electrical and Electronic Engineering, Nanyang Technological University, Singapore, 639798 (e-mail: tguoxin@ntu.edu.sg; ewanghong@ntu.edu.sg).

D.-L. Kwong is with the Institute for Inforcomm Research, Agency for Science, Technology and Research, Singapore, 138632 (e-mail: kwongdl@i2r.a-star.edu.sg).

Color versions of one or more of the figures in this paper are available online at http://ieeexplore.ieee.org.

Digital Object Identifier 10.1109/JSTQE.2018.2811902

fabrication tolerance. Mach-Zehnder Interferometer (MZI) structure, which occupies large footprint, is also adopted to introduce an additional phase to compensate for the phase difference caused by dispersion in the DC [20]–[22]. In addition, adiabatically tapered structure is used for 50:50 power splitting ratio in particular due to its ability of avoiding the coupling between the symmetric and asymmetric mode [23]–[26]. Recently, hybrid plasmonic based WFDC [27], [28] and subwavelength grating (SWG) based WFDC are demonstrated [29], leveraging phase control and effective refractive index (ERI) control respectively. A 5-fold enhancement is achieved in the SWG based WFDC [29]. Nonetheless, the fabrication process is stringent and tedious.

In this paper, we propose and verify a novel mechanism for MIR WFDC based on the physics of rib waveguide dispersion. According to our theoretical analysis, and later verified by the experimental results, such WF mechanism is effective for arbitrary power splitting ratio. Similar to the conventional DC, arbitrary power splitting ratio could be achieved in the rib waveguide MIR WFDC simply by varying the length of the devices, but with significant enhancement in the operation bandwidth. While the devices maintain an average low excess loss of 0.52 $\pm$ 0.18 dB/device, the experimental results show that a 4-fold and a 6-fold enhancement in the operation bandwidth compared to the conventional DC have been achieved in a 6 μm silicon-on-insulator (SOI) WFDC aiming for 100:0 power splitting ratio and in an 18 μm SOI WFDC aiming for 50:50 power splitting ratio respectively in the MIR range of 3.67–3.89 μm. This wavelength range is of particular interests since it covers the fingerprints of carcinogenic gas Formaldehyde (CH_2O), toxic Hydrobromic acid (HBr), corrosive Hydrochloric acid (HCl), and biologically crucial glucose ($C_6H_{12}O_6$), providing an ideal sensing window for these chemicals as it avoids the strong water absorption in 2.7–3.5 μm [30]. The devices are compact with low excess loss and high enhancement in the operation bandwidth compared to the conventional DC. Furthermore, the fabrication process of the devices is CMOS-compatible and extremely simple which utilizes only two etching steps.

II. Concept

A. Theoretical Analysis

In DC, it is the coupling coefficient $\mathrm{C}(\lambda)$ that determines the device's performance [2]. Ideally, $\mathrm{C}(\lambda)$ can be expressed as:

$$\mathrm{C}\left(\lambda\right) = \frac{\pi}{2\mathrm{L}_{\pi}\left(\lambda\right)} \cdots, \tag{1}$$

where λ is the wavelength and $\mathrm{L}_{\pi}(\lambda)$ is the coupling length that permits 100% power transfer from one waveguide to another, i.e., 100:0 power splitting ratio. Thus, $\mathrm{L}_{\pi}(\lambda)$ dominates the performance of the DC. From literature,

$$\mathrm{L}_{\pi}\left(\lambda\right) = \frac{1}{2}\frac{\lambda}{\mathrm{n}_1\left(\lambda\right) - \mathrm{n}_2\left(\lambda\right)} \cdots, \tag{2}$$

where $\mathrm{n}_1(\lambda)$ and $\mathrm{n}_2(\lambda)$ are the dispersive ERI of the symmetric mode and the asymmetric mode in the DC respectively [31]. The percentage change of $\mathrm{L}_{\pi}(\lambda)$ caused by the change of λ can be derived as:

$$\frac{\Delta\mathrm{L}_{\pi}\left(\lambda\right)}{\mathrm{L}_{\pi}\left(\lambda\right)} = \frac{\Delta\lambda}{\lambda} - \frac{\Delta\left(\mathrm{n}_1\left(\lambda\right) - \mathrm{n}_2\left(\lambda\right)\right)}{\mathrm{n}_1\left(\lambda\right) - \mathrm{n}_2\left(\lambda\right)} \cdots, \tag{3}$$

Over a localized wavelength region, the first term is usually negligible. Thus we have the approximation:

$$\frac{\Delta\mathrm{L}_{\pi}\left(\lambda\right)}{\mathrm{L}_{\pi}\left(\lambda\right)} \approx -\frac{\Delta\left(\mathrm{n}_1\left(\lambda\right) - \mathrm{n}_2\left(\lambda\right)\right)}{\mathrm{n}_1\left(\lambda\right) - \mathrm{n}_2\left(\lambda\right)} \cdots, \tag{4}$$

We desire to minimize $\frac{\Delta\mathrm{L}_{\pi}(\lambda)}{\mathrm{L}_{\pi}(\lambda)}$. In the case when $\frac{\Delta\mathrm{L}_{\pi}(\lambda)}{\mathrm{L}_{\pi}(\lambda)} = 0$, $\mathrm{L}_{\pi}(\lambda)$ does not vary with wavelength, and so as $\mathrm{C}(\lambda)$, then the DC performance is independent of wavelength. In Equation (4), $\mathrm{n}_1(\lambda) - \mathrm{n}_2(\lambda)$ is the difference between $\mathrm{n}_1(\lambda)$ and $\mathrm{n}_2(\lambda)$ determined directly by the material and structure of the DC; $\Delta(\mathrm{n}_1(\lambda) - \mathrm{n}_2(\lambda))$ characterizes the sensitivity of $\mathrm{n}_1(\lambda) - \mathrm{n}_2(\lambda)$ to wavelength variation. Mathematically, to realize minimized $\frac{\Delta\mathrm{L}_{\pi}(\lambda)}{\mathrm{L}_{\pi}(\lambda)}$, minimized $\Delta(\mathrm{n}_1(\lambda) - \mathrm{n}_2(\lambda))$ and maximized $\mathrm{n}_1(\lambda) - \mathrm{n}_2(\lambda)$ are desired.

Silicon-on-Insulator (SOI) rib waveguide is employed as a potential candidate to fulfill the above goal since its dispersion could be efficiently engineered by the etching depth D as shown in Fig. 1(a). Additionally, the SOI fabrication process is mature and stable.

The etching depth D in SOI rib waveguide could effectively change the dispersion of the device. Firstly, based on the physics that the mode confinement in Si core is stronger with shallower etch depth D so that the mode possesses higher ERI, both $\mathrm{n}_1(\lambda)$ and $\mathrm{n}_2(\lambda)$ scale up as well as their difference $\mathrm{n}_1(\lambda) - \mathrm{n}_2(\lambda)$ with smaller D. Secondly, in light of the fact that the penetration depth of the evanescent wave into the SiO_2 cladding layer drops as D decreases so that the mode ERI is less affected by wavelength change, $\Delta(\mathrm{n}_1(\lambda) - \mathrm{n}_2(\lambda))$ would decline as D reduces. Hence a conclusion could be reached that rib waveguide WFDC with reduced D achieves better WF performance since $\frac{\Delta\mathrm{L}_{\pi}(\lambda)}{\mathrm{L}_{\pi}(\lambda)}$ is effectively reduced by leveraging greater $\mathrm{n}_1(\lambda) - \mathrm{n}_2(\lambda)$ and smaller $\Delta(\mathrm{n}_1(\lambda) - \mathrm{n}_2(\lambda))$. Additionally, this mechanism for WFDC is realized by varying the structure to control dispersion without targeting at any specific power splitting ratio. Thus, theoretically it works for arbitrary power splitting ratio.

B. Simulation

To thoroughly study the influence of D on the dispersion of rib waveguide WFDC, we perform simulations using Lumerical Mode Solution [32]. The SOI rib waveguide based WFDC has a height of H = 0.4 μm and a waveguide width of W = 1.2 μm. Waveguide with such dimension has been demonstrated with low loss of 2–3 dB/cm over 3.68–3.88 μm in our previous work [30]. The coupling gap of the DC is fixed at 0.5 μm while the etching depth D is the variable. Fig. 2(a) shows the dispersion of $\mathrm{n}_1(\lambda)$ & $\mathrm{n}_2(\lambda)$ in WFDC with different etch depths. It is obvious that both $\mathrm{n}_1(\lambda)$ & $\mathrm{n}_2(\lambda)$ scale up as D decreases. Without loss of generality, from Fig. 2(a), we calculate $\mathrm{n}_1(\lambda) - \mathrm{n}_2(\lambda)$ of devices with different etch depths at three wavelengths, namely 3.68 μm, 3.78 μm, and 3.88 μm; and the result is presented in Fig. 2(b). As D drops from 400 nm to 160 nm, $\mathrm{n}_1(\lambda) - \mathrm{n}_2(\lambda)$

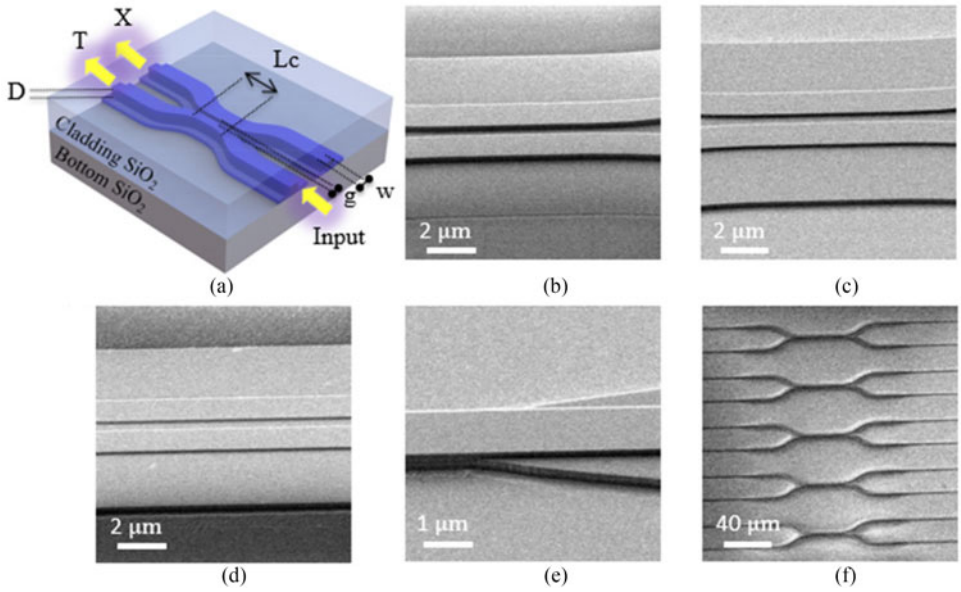

Fig. 1. (a) Schematic of the designed rib waveguide-based WFDC. (b–f) Scanning electron microscope (SEM) image of the fabricated (b) D = 320 nm device, (c) D = 160 nm device, (d) D = 120 nm device, (e) channel waveguide to rib waveguide transition taper of D = 160 nm device, (f) an array of rib waveguide WFDC with different coupling length L_c for various power splitting ratios. The coupling gaps presented in this figure are 500 nm.

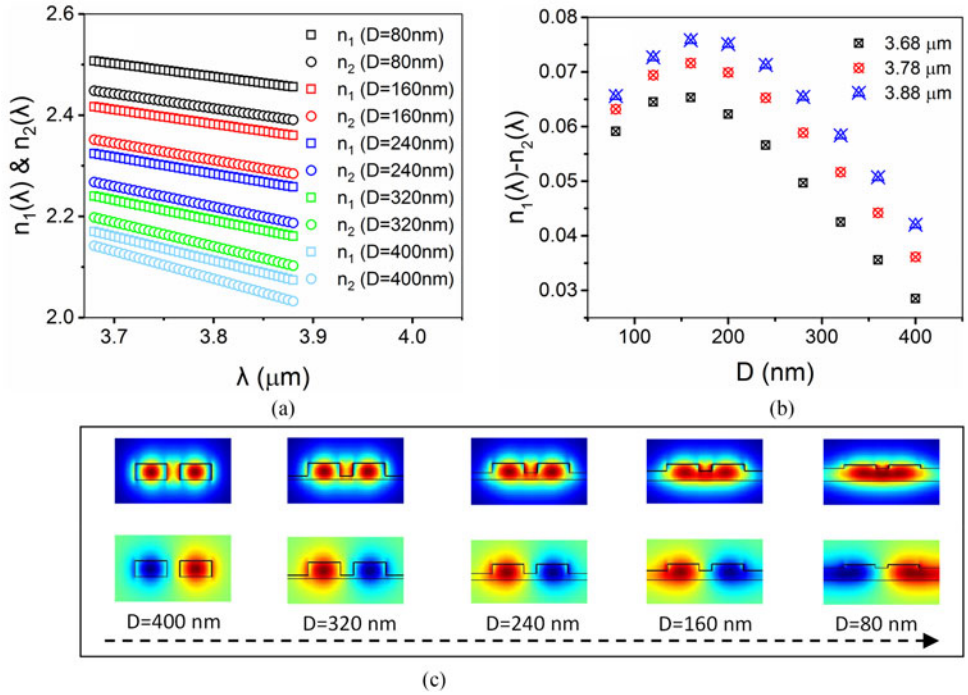

Fig. 2. (a) The dispersion of the symmetric mode ($n_1(\lambda)$) and asymmetric mode ($n_2(\lambda)$), (b) the difference ($n_1(\lambda) - n_2(\lambda)$) at three different wavelength 3.68 μm, 3.78 μm, and 3.88 μm obtained from (a), (c) mode profile of both the symmetric and asymmetric mode in the rib waveguide WFDC with different etch depths.

rises by around 0.035 at all three wavelengths. However, an unexpected decrease in $n_1(\lambda) - n_2(\lambda)$ is observed as D is further reduced from 160 nm to 80 nm. To understand this drop, we perform mode analysis whose result is shown in Fig. 2(c). The electric field (E-field) of the optical modes is strongly confined in the Si ridge at D = 400 nm. As D declines, the mode starts to spread. The symmetric modes spread to the coupling gap while the asymmetric modes to the slabs at the sides. At D = 80 nm, the spread is so strong that the mode behaves more like the fundamental mode in the slab waveguide rather than the symmetric mode in the DC, leading to the unexpected drop.

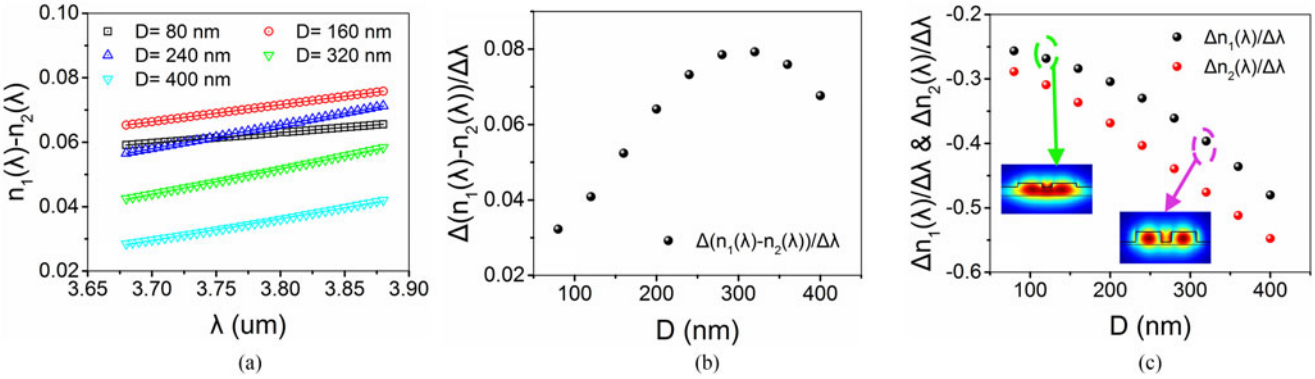

Fig. 3. (a) The dispersion of $(n_1(\lambda) - n_2(\lambda))$, (b) The slope of dispersion of $(n_1(\lambda) - n_2(\lambda))$ with respect to (w.r.t) λ, (c) The slope of dispersion of $n_1(\lambda)$ and $n_2(\lambda)$ individually w.r.t λ in the rib waveguide WFDC with different etch depths. The inset in (c) shows the mode profile of the symmetric mode in D = 120 nm and D = 320 nm devices respectively.

To study $\Delta(n_1(\lambda) - n_2(\lambda))$, we simulate the dispersion of $n_1(\lambda) - n_2(\lambda)$ in WFDC with different etch depths. The result is presented in Fig. 3(a). The slope of the dispersion, which characterizes the sensitivity of $n_1(\lambda) - n_2(\lambda)$ due to wavelength variation would represent $\Delta(n_1(\lambda) - n_2(\lambda))$. Fig. 3(a) indicates that $n_1(\lambda) - n_2(\lambda)$ generally rises as D declines except at D = 80 nm. This further strengthens our previous claim that the rib structure behaves slab waveguide-like rather than DC-like at D = 80 nm. We plot the slope of the dispersion of $n_1(\lambda) - n_2(\lambda)$ in Fig. 3(b). From D = 320 nm to D = 80 nm, the slope decreases as D drops. Nevertheless, an abnormal fall is observed when D is greater than 320 nm. We examine the slope of the dispersion of $n_1(\lambda)$ and $n_2(\lambda)$ individually to understand this drop. The result is plotted in Fig. 3(c). It is shown that the slope of the dispersion of $n_2(\lambda)$ decreases almost linearly throughout the whole range between D = 80 nm and D = 400 nm while the drop of the slope of the dispersion of $n_1(\lambda)$ is slow at D = 80 nm, accelerates as D increases, and finally reaches the same rate as that of $n_2(\lambda)$. The difference between the slope of the dispersion of $n_1(\lambda)$ and $n_2(\lambda)$ could be attributed to the fact that the symmetric mode has some E-field strongly confined in the gap Si region while the asymmetric mode does not, as can be revealed from Fig. 2(c) D = 80 nm. The Si gap region which possesses a large refractive index of around 3.4 maintains the high ERI so that $n_1(\lambda)$ decreases slower than $n_2(\lambda)$ at small D. At larger D, the E-field confinement of the symmetric mode in the Si gap region is weaker as shown in the insets of Fig. 3(c), meaning that the influence of the Si gap region is much weaker at D = 320 nm compared to at D = 120 nm. Therefore, the reduction rate of the slope of the dispersion of $n_1(\lambda)$ increases and approaches that of $n_2(\lambda)$ as D rises.

III. Device Fabrication and Characterization

We design and fabricate rib waveguide WFDCs with different etch depths in order to show their WF effect. Without loss of generality, Fig. 1(b)–(d) shows the coupling region of devices with D = 320 nm, 160 nm, and 120 nm respectively. The slab width is 7 μm for all the designs. The waveguide cross section is the same as in the simulation. As shown in Fig. 1(e), transition tapers tapering from 1.2 μm to 7.2 μm with a length of 18 μm are used to convert the channel waveguide mode to rib waveguide mode in order to prevent larger mode mismatch and strong reflection. Arrays of WFDCs with different coupling length L_c from 0 μm to 48 μm in step of 3 μm are fabricated to achieve arbitrary power splitting ratio (see Fig. 1(f)).

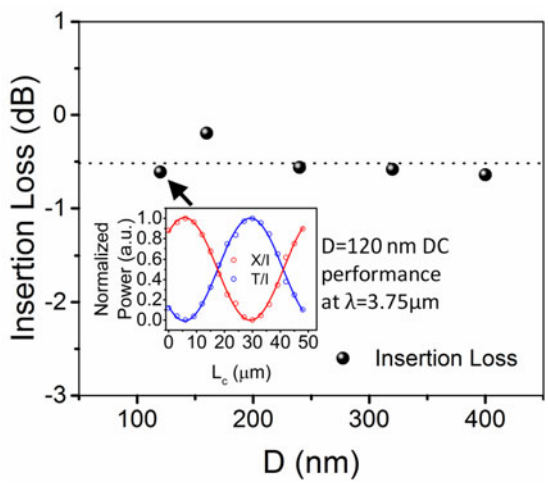

Fig. 4. Average insertion loss of the fabricated devices in 3.67 μm–3.89 μm. The inset shows the directional coupler behavior of D = 120 nm device at 3.75 μm.

The fabrication starts with a commercially available 8-inch SOI wafer with 220 nm device layer. 180 nm Si is epitaxially grown to extend the device layer thickness to 400 nm to meet the MIR requirement. SiO_2 is deposited as the hard mask, followed by deep ultra-violet (DUV) photolithography for patterning. Two-step Si reactive ion etching (RIE) is performed for device definition. 3 μm SiO_2 is deposited using plasma enhanced chemical vapour deposition (PECVD) to form the cladding layer. Lastly, around 100 μm deep trench is formed for butt fiber coupling testing. The testing setup is described in our previous work [3].

Figs. 4–6 shows the experimental results. The insertion loss of the WFDCs with different etch depths is presented in Fig. 4. An average insertion loss of −0.52 dB in 3.67 μm–3.89 μm is

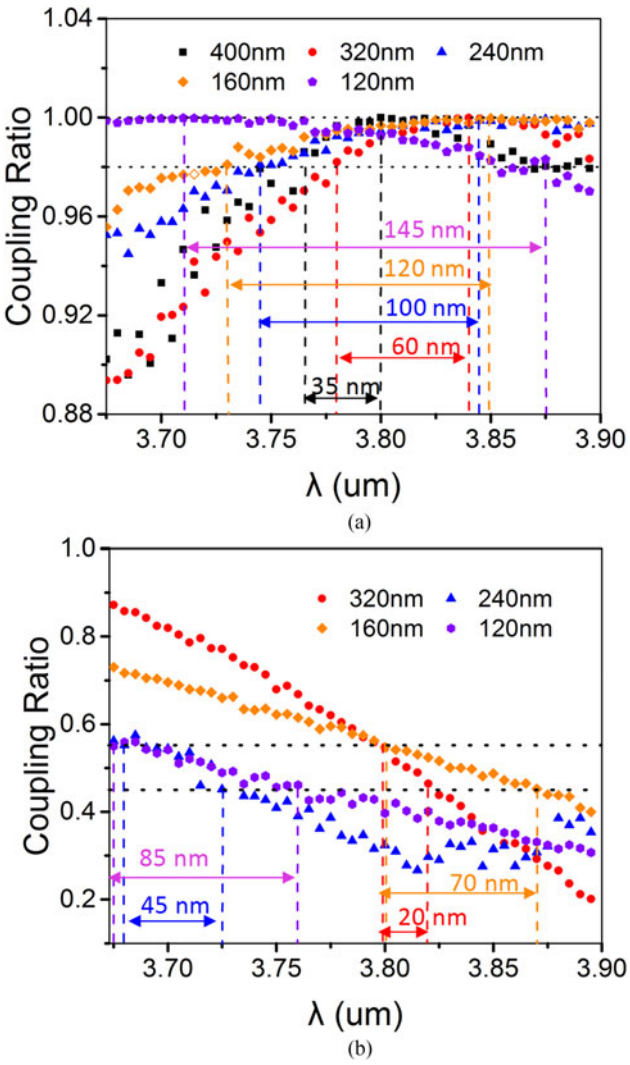

Fig. 5. The performance of WFDC across 3.67–3.89 μm in devices with different etch depths aiming at (a) 100:0 (b) 50:50 power splitting ratio. The coupling length of each device in (a) is: (D = 400 nm, L_c = 49 μm), (D = 320 nm, L_c = 30 μm), (D = 240 nm, L_c = 21 μm), (D = 160 nm, L_c = 6 μm), (D = 120 nm, L_c = 6 μm); in (b) is (D = 320 nm, L_c = 36 μm), (D = 240 nm, L_c = 42 μm), (D = 160 nm, L_c = 18 μm), (D = 120 nm, L_c = 18 μm).

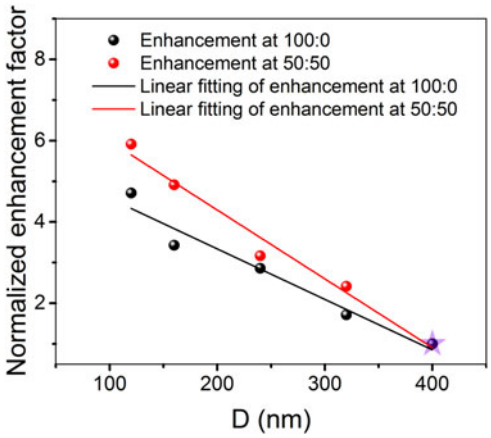

Fig. 6. The normalized enhancement factor in devices with different etch depths derived from Fig. 5.

measured with a variance of 0.18 dB. Meanwhile, the propagation loss of the waveguide is maintained at 2–3 dB/cm over 3.67–3.89 μm, which is consistent with our previous results. To ensure that the D = 120 nm device is working as a WFDC rather than a slab waveguide, we measured the normalized transmission (T/I) and crossing (X/I) power at several L_c where the result is shown in the inset of Fig. 4. According to our previously proposed model [3], T and X should follow

$$\frac{T}{I} = t^2 = \cos^2\left(\frac{\pi}{2}\frac{L_c}{L_\pi} + \varnothing_0\right)\ldots \tag{5}$$

$$\frac{X}{I} = K^2 = \sin^2\left(\frac{\pi}{2}\frac{L_c}{L_\pi} + \varnothing_0\right)\ldots \tag{6}$$

in DCs, where T is the power transmitted through the input waveguide, X is the power coupled evanescently through the DC, I = X + T is the total power in the directional coupler, t and K are the power transmission coefficient and power coupling coefficient respectively, and $\varnothing_0$ is the initial phase introduced by the S bends before the coupling region. The sine squared fitting of X/I and T/I shows an Adj. R-square of 0.99, proving the good DC performance of the D = 120 nm device. The large X at L_c = 0 μm shows significant coupling in the S-bend region which agrees with our previously proposed model. The devices with larger D maintain the good DC performance as the devices behave less like slab waveguide.

Fig. 5 shows the WFDC performance for 100:0 and 50:50 power splitting ratio in order to indicate its superior WF performance as well as the feasibility and simplicity of the novel mechanism to work for arbitrary power splitting ratio without loss of generality. The WFDC's performance for 100:0 power splitting ratio is shown in Fig. 5(a). L_c = 49 μm WFDC with D = 400 nm and L_c = 6 μm WFDC with D = 120 nm could achieve 100:0 power splitting ratio in the range of 3.67–3.89 μm. The acceptance range is defined as 100:0–98:2. The upper limit and lower limit of 100:0–98:2 region is the wavelength with the highest coupling ratio and the last wavelength that stays in this region respectively. It is demonstrated in Fig. 5(a) that as D drops from 400 nm to 120 nm in step of 80 nm, the bandwidths of 100:0-98:2 region are 35 nm, 60 nm, 100 nm, 120 nm, and 145 nm. A highest enhancement of more than 4-fold in operation bandwidth is achieved in D = 120 nm rib waveguide WFDC compared with the conventional DC.

The WFDC's performance for 50:50 power splitting ratio is shown in Fig. 5(b). L_c = 36 μm WFDC with D = 320 nm and L_c = 18 μm WFDC with D = 120 nm could achieve 50:50 power splitting ratio in the range of 3.67–3.89 μm. The acceptance range is defined as 45:55–55:45, which is similar to [28]. The upper limit and lower limit of 45:55–55:45 region are defined as the two last wavelengths that stay in the region. It is revealed in Fig. 5(b) that as D decreases from 320 nm to 120 nm in step of 80 nm, the bandwidths of 45:55–55:45 region are 20 nm, 45 nm, 70 nm, and 85 nm. D = 400 nm WFDC is not presented here because the L_c of the designed device is not long enough to get a downward 50:50 power splitting ratio as the rest of devices with smaller etch depths do.

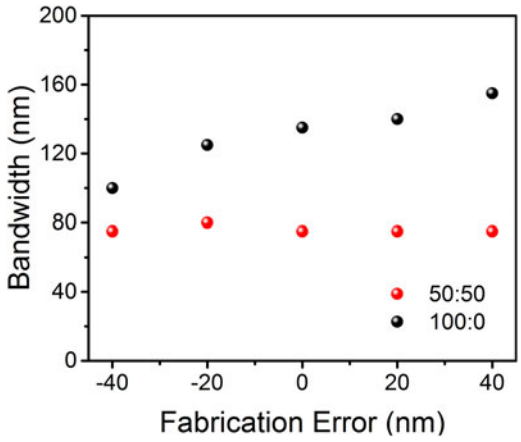

Fig. 7. The simulation result of the bandwidth of WFDC (D = 120 nm) with respect to fabrication errors. 50:50 power splitting ratio is less vulnerable to fabrication tolerance while 100:0 requires more precise fabrication control.

The normalized enhancement factor is defined as the ratio of the broadened bandwidth to the bandwidth of the conventional DC with etch depth of 400 nm. From the results shown in Fig. 5(a), we calculate the normalized enhancement factor at 100:0. The result is presented as black dots in Fig. 6. An enhancement factor of more than 4-fold could be achieved with D = 120 nm WFDC at 100:0 power splitting ratio. A linear fitting of the normalized enhancement factor shows an Adj. R-Square of 0.98, showing a reasonably good linear relationship between the normalized enhancement factor and the etch depth D. Under the assumption of such linear relationship, we find the gradient of the enhancement factor at 50:50 normalized to D = 320 nm device with respect to etch depth by linear fitting. The linear fitting shows an Adj. R-Square of 0.97. We then extrapolate the corresponding normalized enhancement factor for D = 400 nm, and finally shift the linear curve up so that the normalized enhancement factor at D = 400 nm is 1, which is marked by the purple star. After such mathematical manipulation, an enhancement factor of around 6-fold is projected for D = 120 nm WFDC at 50:50 power splitting ratio.

The fabrication tolerance of our design is investigated by 3D FDTD simulation [33]. The fabrication error is defined as $\Delta_{fab} = 2\Delta_{Gap} = -2\Delta_{WG}$, where Δ_{Gap} and Δ_{WG} describe the coupling gap variation and waveguide width variation respectively according to [34]. As shown in Fig. 7, for 50:50 power splitting ratio WFDC, the fabrication error of ± 40 nm only causes the maximum bandwidth variation of $+6.7\%$. Meanwhile, with the same range of fabrication error, the 100:0 power splitting WFDC has a slightly higher variation around -25% to $+15\%$. This deteriorated fabrication tolerance could be attributed to that WFDC behaves slab waveguide-like with small coupling gap, which disturbs 100:0 power splitting ratio yet serves as a Y–junction to realize 50:50 power splitting ratio. Thus, to improve the fabrication tolerance of WFDC for non-50:50 power splitting ratio, larger coupling gap is desired.

Table I shows the performance of the recently demonstrated WFDC for comparison. By leveraging the novel mechanism based on rib waveguide dispersion engineering, our compact devices of <20 μm in length realize high enhancement factor in operation bandwidth compared to the conventional DC while maintaining the lowest excess loss. In addition, our WFDC is the first WFDC demonstrated for MIR application.

TABLE I
RECENTLY DEMONSTRATED WFDC PERFORMANCE

No	Mechanism	Length (μm)	Excess loss (dB)	λ (μm)	Enhancement factor at 50:50	Ref
1	Asymmetry	7.4	N.A.	~1.55	~7	[19]
2	MZI	10^4	~2.8	~1.55	~3	[22]
3	Adiabatic	>100	~2	~1.55	~4	[26]
4	Hybrid plasmonic	21.2	0.89	~1.55	~4	[28]
5	SWG	19.2	~0.7	~1.55	~5	[29]
6	Rib WG dispersion engineering (this work)	<20	0.52	~3.78	~6	N.A.

IV. CONCLUSION

In summary we proposed a novel mechanism by analyzing the physics behind the dispersion of rib waveguide DC to achieve MIR WFDC. The MIR WFDC achieved by rib waveguide dispersion engineering is CMOS-compatible, compact, and effective in a broadband range with low excess loss. Meanwhile, based on the novel mechanism, arbitrary power splitting ratio could be achieved in the WFDC simply by varying the length of the devices. A prominent 6-fold and a 4-fold enhancement are demonstrated for 50:50 (± 5) and 100:0 (-2) power splitting ratio respectively in devices less than 20 μm while the loss is maintained as low as -0.52 ± 0.18 dB/device. These MIR WFDCs are promising to be incorporated into the MIR spectrometer sensing systems which require broadband components. Furthermore, the proposed novel mechanism could be utilized in NIR WFDC as well to realize better performance.

REFERENCES

[1] T. Hu *et al.*, "Silicon photonic platforms for mid-infrared applications [Invited]," *Photon. Res.*, vol. 5, no. 5, pp. 417–430, 2017.
[2] G. B. Rieker *et al.*, "Frequency-comb-based remote sensing of greenhouse gases over kilometer air paths," *Optica*, vol. 1, no. 5, pp. 290–298, 2014.
[3] G. Mi, C. Horvath, M. Aktary, and V. Van, "Silicon microring refractometric sensor for atmospheric CO2 gas monitoring," *Opt. Express*, vol. 24, no. 2, pp. 1773–1780, 2016.
[4] Y. Chen, H. Lin, J. Hu, and M. Li, "Heterogeneously integrated silicon photonics for the mid-infrared and spectroscopic sensing," *ACS Nano*, vol. 8, no. 7, pp. 6955–6961, 2014.
[5] P. T. Lin *et al.*, "Chip-scale mid-infrared chemical sensors using air-clad pedestal silicon waveguides," *Lab Chip*, vol. 13, no. 11, pp. 2161–2166, 2013.
[6] G. Z. Mashanovich *et al.*, "Silicon photonic waveguides and devices for near-and mid-IR applications," *IEEE J. Sel. Topics Quantum Electron.*, vol. 21, no. 4, Jul./Aug. 2015, Art. no. 8200112.
[7] V. Singh *et al.*, "Mid-infrared materials and devices on a Si platform for optical sensing," *Sci. Technol. Adv. Mater.*, vol. 15, no. 1, 2014, Art. no. 14603.
[8] P. T. Lin *et al.*, "Label-free glucose sensing using chip-scale mid-infrared integrated photonics," *Adv. Opt. Mater.*, vol. 4, no. 11, pp. 1755–1759, 2016.
[9] F. Dell'Olio and V. M. N. Passaro, "Optical sensing by optimized silicon slot waveguides," *Opt. Express*, vol. 15, no. 8, pp. 4977–4993, 2007.
[10] C. A. Barrios *et al.*, "Slot-waveguide biochemical sensor," *Opt. Lett.*, vol. 32, no. 21, pp. 3080–3082, 2007.

[11] A. H. J. Yang *et al.*, "Optical manipulation of nanoparticles and biomolecules in sub-wavelength slot waveguides," *Nature*, vol. 457, no. 7225, pp. 71–75, 2008.

[12] H. Subbaraman *et al.*, "Recent advances in silicon-based passive and active optical interconnects," *Opt. Express*, vol. 23, no. 3, pp. 2487–2511, 2015.

[13] M. Stegmaier and W. H. P. Pernice, "Broadband directional coupling in aluminum nitride nanophotonic circuits," *Opt. Express*, vol. 21, no. 6, pp. 7304–7315, 2013.

[14] P. Splitters, "Broad-band optical directional couplers and polarization splitters," *J. Lightw. Technol.*, vol. 7, no. 6, pp. 925–930, Jun. 1989.

[15] A. Takagi, K. Jinguji, and M. Kawachi, "Broadband silica-based optical waveguide coupler with asymmetric structure," *Electron. Lett.*, vol. 26, no. 2, pp. 132–133, 1990.

[16] J. D. Love and V. V. Steblina, "Highly broadband buried channel couplers," *Electron. Lett.*, vol. 30, no. 22, pp. 1853–1855, 1994.

[17] Y. Emori, T. Mizumoto, and Y. Naito, "Design of wavelength-flattened coupler using a novel diagram," *J. Lightw. Technol.*, vol. 14, no. 12, pp. 2677–2683, 1996.

[18] C. R. Doerr *et al.*, "Bending of a planar lightwave circuit $2 * 2$ coupler to desensitize it to wavelength, polarization, and fabrication changes," *IEEE Photon. Technol. Lett.*, vol. 17, no. 6, pp. 1211–1213, Jun. 2005.

[19] H. Morino, T. Maruyama, and K. Iiyama, "Reduction of wavelength dependence of coupling characteristics using si optical waveguide curved directional coupler," *J. Lightw. Technol.*, vol. 32, no. 12, pp. 2188–2192, Jun. 2014.

[20] B. E. Little, T. Murphy, and S. Member, "Design rules for maximally flat wavelength-insensitive optical power dividers using Mach–Zehnder structures," *IEEE Photon. Technol. Lett.*, vol. 9, no. 12, pp. 1607–1609, Dec. 1997.

[21] Q. Wang and S. He, "Optimal design of planar wavelength circuits based on Mach–Zehnder interferometers and their cascaded forms," *J. Lightw. Technol.*, vol. 23, no. 3, pp. 1284–1290, Mar. 2005.

[22] S. Hsu, "Optical waveguide tap with low polarization dependence and flattened wavelength using a Mach–Zehnder directional coupler," *Appl. Opt.*, vol. 49, no. 13, pp. 2434–2440, 2010.

[23] C. P. Hussell, R. V Ramaswamy, R. Srivastava, and J. L. Jackel, "Wavelength and polarization insensitive 3 dB cross-coupler power dividers by ion exchange in glass," *Appl. Phys. Lett.*, vol. 2381, no. 1990, pp. 4–7, 2016.

[24] Y. Shani *et al.*, "Integrated optic adiabatic devices on silicon," *IEEE J. Quantum Electron.*, vol. 27, no. 3, pp. 556–566, Mar. 1991.

[25] R. Adar, C. H. Henry, R. F. Kazarinov, R. C. Kistler, and G. R. Weber, "Adiabatic 3-dB couplers, filters, and multiplexers made with silica waveguides on silicon," *J. Lightw. Technol.*, vol. 10, no. 1, pp. 46–50, 1992.

[26] H. Yun, W. Shi, Y. Wang, L. Chrostowski, and N. A. F. Jaeger, "$2 * 2$ Adiabatic 3-dB coupler on silicon-on-insulator rib waveguides," *Proc. SPIE*, vol. 8915, pp. 2–7, 2013.

[27] M. Z. Alam, J. N. Caspers, J. S. Aitchison, and M. Mojahedi, "Compact low loss and broadband hybrid plasmonic directional coupler," *Opt. Express*, vol. 21, no. 13, pp. 3371–3373, 2013.

[28] J. N. Caspers and M. Mojahedi, "Measurement of a compact colorless 3 dB hybrid plasmonic directional coupler," *Opt. Lett.*, vol. 39, no. 11, pp. 3262–3265, 2014.

[29] R. Halir, P. Cheben, D. Xu, J. H. Schmid, and S. Janz, "Colorless directional coupler with dispersion engineered sub-wavelength structure," *Opt. Express*, vol. 20, no. 12, pp. 515–517, 2012.

[30] B. Dong *et al.*, "Silicon-on-insulator waveguide devices for broadband mid-infrared photonics silicon-on-insulator waveguide devices," *IEEE Photonics J.*, vol. 9, no. 3, Jun. 2017, Art. no. 4501410.

[31] R. R. A. Syms and J. R. Cozens, *Optical Guided Waves and Devices*, 1st ed. Berkshire, MA, USA: McGraw-Hill, 1992.

[32] "Evanescent waveguide couplers | Lumerical Knowledge Base," 2016. [Online]. Available: https://kb.lumerical.com/en/pic_passive_waveguide_couplers_evanescent.html#results. Accessed on: Oct. 26, 2016.

[33] "Lumerical solutions, inc. | innovative photonic design tools," [Online]. Available: https://www.lumerical.com/. Accessed on: Dec. 28, 2017.

[34] A. Prinzen, M. Waldow, and H. Kurz, "Fabrication tolerances of SOI based directional couplers and ring resonators," *Opt. Express*, vol. 21, no. 14, pp. 21–26, 2013.

Bowei Dong (S'17) was born in Xiamen, Fujian, China, in 1992. He received the B.S. degree in physics with second major in mathematics from the Nanyang Technological University, Singapore, in 2015 where he is currently working toward the Ph.D. degree. His research interests include waveguides, integrated silicon photonics, and integrated mid-infrared photonics for sensing and healthcare applications.

Xianshu Luo received the B. E. degree in microelectronics from Jilin University, Changchun, Jilin, China, in 2003, the M.S. degree in microelectronics and solid state physics from Institute of Semiconductors, Chinese Academy of Sciences, Beijing, China, in 2006, and the Ph.D. degree in electrical and computer engineering from The Hong Kong University of Science and Technology, Hong Kong, in 2010.

His Ph.D. work covered a broad range subject to silicon micro/nanophotonics for networks-on-chip applications. He is currently a Scientist with the Institute of Microelectronics, Agency for Science, Technology and Research, Singapore, where he is engaged in research on silicon photonic integrated circuits and heterogeneous integration of optoelectronic integrated circuits for various applications.

Dr. Luo received the IEEE Photonics Society Best Student Paper Award in the 14th OptoElectronics and Communications Conference in 2009.

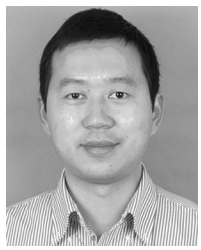

Ting Hu received the B. E. and M. S. degrees in microelectronics from Xi'an University of Technology, Xi'an, China, in 2006 and 2010, respectively, and the Ph.D. degree in microelectronics from Zhejiang University, Hangzhou, China, in Mar. 2014. From 2014 to 2016, he worked successively with the University of Ottawa and the Nanyang Technological University as a Research Fellow. He is currently working with the Institute of Microelectronics, Agency for Science, Technology and Research, Singapore. He has authored and coauthored more than 30 peer-reviewed journal papers. His research interests include the design, fabrication, and characterization of silicon photonic devices working at the near- and mid-infrared wavelengths.

Tina Xin Guo received the M.S. degree in engineering from Nanyang Technological University, Singapore, in 2001. She is currently working with the Silicon Technologies, Centre of Excellence, Nanyang Technological University, Singapore.

Hong Wang received the B.Eng. degree from Zhejiang University, Hangzhou, China, in 1988, and the M.Eng. and Ph.D degrees from the Nanyang Technological University, Singapore, in 1998 and 2001, respectively. From 1988 to 1994, he was with the Institute of Semiconductors, Chinese Academy of Sciences. From 1994 to 1995, he was a Royal Research Fellow with the British Telecommunications Laboratories, Ipswich, U.K., where he was involved with the development of InP-based heterostructure field-effect transistors (HFETs) using E-beam lithography. Since 1996, he has been with Nanyang Technological University, where he is currently an Associate Professor, and Director of Nanyang NanoFabrication Centre (N2FC). He has authored or coauthored more than 230 technical papers. He was the recipient of the 2007 Defence Technology Prize, Ministry of Defence, Singapore. He served as a Session Chair, and Sub-Committee Member for 2009 and 2010 IEDM.

Dim-Lee Kwong (F'09) received the B.S. degree in physics and the M.S. degree in nuclear engineering from the National Tsing Hua University, Hsinchu, Taiwan, in 1977 and 1979, respectively, and the Ph.D. degree in electrical engineering from Rice University, Houston, TX, USA, in 1982.

He is the Executive Director of the Institute for Infocomm Research, Agency for Science, Technology and Research, Singapore, and a Professor of electrical and computer engineering with the National University of Singapore. He was the Executive Director with the Institute of Microelectronics from 2005–2016, the Earl N. and Margaret Bransfield Endowed Professor with the University of Texas at Austin from 1990–2007 and a Temasek Professor at NUS from 2001 to 2004. He has authored or coauthored more than 1100 refereed archival publications, delivered more than 100 plenary, keynote and invited talks at international conferences, and had more than 25 U.S. patents granted. More than 60 students have received the Ph.D. degrees under his supervision.

Dr. Kwong was the recipient of the IBM Faculty Award for 1984–86, Semiconductor Research Corporation Inventor Awards in 1993 and 1994, Halliburton Foundation Research Award in 1994, Engineering Foundation Outstanding Teaching Award in 1995, IEEE George Smith Award in 2007, and the 2011 IEEE Frederik Philips Award with citation: "For leadership in silicon technology and excellence in the management of microelectronics R&D." He holds the role of Special Advisor on the Asia-Pacific Leadership Council of Global Semiconductor Alliance and serves on the Board of Advisors of Singapore Semiconductor Industry Association.

Patrick Guo-Qiang Lo received the M.S. and Ph.D. degrees in electrical and computer engineering from the University of Texas at Austin, Austin, TX, USA, in 1989 and 1992, respectively.

He was with the Integrated Device Technology, Inc., both in San Jose, CA, USA, and Hillsboro, OR, USA, from 1992 to 2004. He was involved in CMOS technology areas in process and integration research and development. Since 2004, he has been with the Institute of Microelectronics/A∗STAR, Singapore, where he is currently the Program Director of the Nanoelectronics and Photonics Program and TSV (through-silicon-via) Taskforce. His current research interests include novel semiconductor device and integration technology, in the areas of nanoelectronics, silicon photonics, GaN-on-silicon-based power electronics and also emerging memories, particularly in the paths toward to productization and commercialization. He has authored or coauthored more than 200 peer-reviewed journal and conferences publications, and holds more than 30 granted patents.

Dr. Lo was the recipient of the IEEE George E. Smith Award in 2008 for the best paper published in the IEEE ELECTRONIC DEVICE LETTERS in 2007, and two times recipient of Singapore's National Technology Award in 2008 and President Technology Award in 2010.

Chengkuo Lee (S'93–M'96) received the M.S. degree in materials science and engineering from National Tsing Hua University, Hsinchu, Taiwan, in 1991, the M.S. degree in industrial and system engineering from Rutgers University, New Brunswick, NJ, USA, in 1993, and the Ph.D. degree in precision engineering from the University of Tokyo, Tokyo, Japan, in 1996.

He was a Foreign Researcher with the Nanometerscale Manufacturing Science Laboratory, the Research Center for Advanced Science and Technology, University of Tokyo, from 1993 to 1996. He had also worked with the Technical Engineering Laboratory, Advanced Industrial Science and Technology, Ministry of International Trade and Industry of Japan, as a Japan Science and Technology Research Fellow, in 1996. Thereafter, he was a Senior Research Staff Member of the Microsystems Laboratory, Industrial Technology Research Institute, Hsinchu. In September 1997, he joined the Metrodyne Microsystem Corporation, Hsinchu, and established the MEMS Device Division and the first micromachining laboratory for commercial purposes in Taiwan. He was the Manager with the MEMS Device Division between 1997 and 2000. He was an Adjunct Assistant Professor with the Department of Electrophysics, National Chiao Tung University, Hsinchu, Taiwan, in 1998, and an Adjunct Assistant Professor with the Institute of Precision Engineering, National Chung Hsing University, Taichung, Taiwan, from 2001 to 2005. He cofounded Asia PacificMicrosystems, Inc. (APM), Hsinchu, in August 2001, and he became the Vice President of R&D; then, later, until the end of 2005, he became the Vice President of the optical communication business unit and the Special Assistant to the Chief Executive Officer in charge of international business and technical marketing for MEMS foundry service at APM, Inc., one of the top 30 MEMS manufacturers in the world in 2004. From 2006 to 2009, he was a Senior Member of Technical Staff with the Institute of Microelectronics, Agency for Science, Technology and Research, Singapore. He is currently an Associate Professor with the Department of Electrical and Computer Engineering, and Director of Center for Intelligent Sensors and MEMS at National University of Singapore, Singapore. He is the coauthor of the book *Advanced MEMS Packaging* (McGraw-Hill, 2010). He has authored or coauthored more than 300 international Conference papers and extended abstracts, 250 peer-reviewed international journal articles, and nine U.S. patents in the MEMS, NEMS, metamaterials, nanophotonics, and nanotechnology fields.